Detection of infill wall damage due to earthquakes from vibration data

Detection of infill wall damage due to earthquakes from vibration data

Vanni Nicoletti[a1], Davide Arezzo[a], Sandro Carbonari[a], Fabrizio Gara[a]

[a] Dept. of Construction, Civil Engineering and Architecture (DICEA), Università Politecnica delle Marche, Via Brecce Bianche, 60131 Ancona, Italy.

E-mail: v.nicoletti@pm.univpm.it; d.arezzo@pm.univpm.it; s.carbonari@univpm.it; f.gara@univpm.it

Abstract

Vibration-based methodologies are nowadays gaining increasing application for the structural health monitoring and damage detection on buildings, especially damage due to earthquakes. A fast and efficient damage detection on structural and non-structural components can support the decision making process after exceptional events and may contribute to reduce troubles due to the inoccupancy of buildings.

The paper offers insights on the usefulness of vibration data for the damage detection in infilled frame structures starting from the tracking of the stiffness and modal properties of an infilled laboratory steel-concrete composite mock-up subjected to vibration-based tests. The mock-up has been object of an extensive experimental campaign that involved both quasi-static cyclic and dynamic tests characterized by different level of excitation provided to the structure. Cyclic load tests are performed to simulate the effects of earthquakes by progressively increasing the imposed displacement to the cracking and then to the failure of infills. The dynamic tests are executed at the various steps to capture the effects of the infill damage on the global dynamic response triggered by excitations of different amplitudes. Results of dynamic and quasi-static tests are used to correlate the infill damage with the mechanical properties and the modal parameters of the mock-up, as well as with the vibration amplitude, providing information about the damage expected during low and moderate seismic events as a function of the registered dynamic response of the building by structural health monitoring systems.

Keywords: earthquake damage, infill damage detection, laboratory experimentation, structural health monitoring, vibration-based tests, cyclic load test.

1. Introduction

The safety assessment of buildings and infrastructures after earthquakes is of paramount importance for the management of the post-earthquake emergency; indeed, a fast and efficient damage evaluation of structural and non-structural members of buildings may contribute to reduce social hardships and economic losses due to displaced people. Post-earthquake building inspections are needed before structures can be accessible again, and are usually performed by technicians starting from the epicentral area. Unfortunately, these operations take a long time due to the high number of constructions and the limited number of technicians. Structural Health Monitoring (SHM) systems can contribute to face this issue by providing information about the building health status after exceptional events, such as earthquakes, hurricanes, blasts, vehicle impacts, etc. In addition, SHM permits to get (often continuously) information about some features of the structure during the life cycle (e.g., modal parameters, crack opening, sub-component tilting), from which also ageing effects can be controlled (e.g., material deterioration, corrosion, etc.). If the SHM system reports alert situations through suitably installed specific sensors, visual inspections can be also performed to identify damage on structural and non-structural elements, and destructive or non-destructive experimental tests can be executed as well to evaluate the residual material mechanical properties. For strategic structures with public functions (e.g., bridges, hospitals, police and fire stations, schools, etc.), the SHM is recommended in view of their relevance in the post disaster management.

Among SHM systems, the structural dynamic monitoring is nowadays widely adopted worldwide since it is rather easy to be conceived and does not require the interruption of the activities, neither for the installation nor for the data acquisition. Also, the structure is commonly excited by the surrounding environment (e.g., anthropic activities, ambient noise, microtremors and earthquakes), therefore a specific excitation is not required to be furnished to the structure. The dynamic monitoring is based on the use of vibration-based methods that adopt accelerations or velocities measured over the structure to characterize its dynamics, in terms of modal parameters, namely resonant frequencies, mode shapes and modal damping ratios. The basic idea behind this methodology is that modal parameters vary with the health status of the building

[1] Corresponding author: Department of Construction, Civil Engineering and Architecture (DICEA), Università Politecnica delle Marche, Via Brecce Bianche, 60131 Ancona, Italy - E-mail address: v.nicoletti@pm.univpm.it

(i.e., with the presence and/or the evolution of damage) since they are functions of the structure physical properties (mass, damping, and stiffness)[1]. Therefore, damage or changes of material mechanical properties and boundary conditions will cause changes in the modal properties, which can be detected performing dynamic tests on the structure over time.

A comprehensive literature review about vibration-based methods for damage detection can be found in [1-3]. Among them, the response-based methods are the most adopted ones, even if they present some challenges in real building applications [4] related to the location and the extent of damage (detection of structural and/or non-structural damaged components), the sensitivity of the dynamic response to damage, the choice of damage indexes to be used, the sensor locations, etc. However, although this strategy is widely recognised to be of useful application, a relatively low number of works can be found dealing with applications on real or scaled structures. Some authors performed vibration-based tests on real buildings during the gradual artificially induced damage to both structural and non-structural components [5-7] or due to earthquakes [8,9], while others investigated the modal property evolutions of laboratory specimens representative of Reinforced Concrete (RC) [10-14], steel [15,16], and steel-concrete composite structures [4,17] subjected to displacements and forces such as to produce structural and non-structural damage. However, a lack of works dealing with damage evaluation of infilled structures by using vibration-based techniques can be observed in the literature.

In framed RC and steel buildings, infills are the most important non-structural elements that may affect the structural dynamic response [3,18] and the seismic performance [19-23], sometimes leading to the development of undesirable effects, such as the activation of soft storey mechanisms or the shear failure of short unconfined columns [24,25]. Thus, not only damage to structural elements but also to non-structural components often reflects in changes on the dynamic behaviour of infilled structures, as proved by some authors that investigated the dynamic response of infilled buildings after damage produced by earthquakes all around the world [26-30]. These variations are mainly due to the stiffness degradation of members since the mass remains almost the same [31-33]. Unfortunately, differentiating between damage occurred to structural and non-structural members is a hard task, especially when tests are performed on the whole building with infills. At the same time, it is crucial to establish if a structure can be further used or not after an exceptional event, by eventually repairing the light damage occurred to non-structural components to prevent risks during aftershocks. An in-depth knowledge of the building dynamics can support the identification of damage occurred to structural and non-structural components. As example, vibration-based tests performed during the building construction allow to gather modal parameters of the bare frame as well as those of the infilled structure, and may contribute to define thresholds useful to distinguish between structural and non-structural damage. Above strategy is proposed in [34], but very few works are available in the literature dealing with applications to real or scaled structures, focusing on dynamic tests performed on both bare, infilled, and damaged infilled frames. Thus, further studies on the application of vibration-based tests for the damage detection in infilled structures are necessary, addressing issues such as the possibility to identify non-structural damage and to establish the usefulness of vibration data obtained from SHM systems.

This paper discusses the usefulness of vibration data for the damage detection in infilled frame structures starting from results of vibration-based tests on an infilled laboratory steel-concrete composite mock-up. The study is based on results of a laboratory experimental campaign, which includes quasi-static and dynamic tests performed on a laboratory mock-up. Quasi-static tests are designed to induce a step-by-step progressive damage to infills simulating an earthquake damage scenario, meanwhile different types of dynamic tests are performed on the undamaged and damaged structure to evaluate the response of the system subjected to different level of excitation. Tests are designed to preserve the structural elements in the linear range, and results provide useful information for the detection and tracking of damage to non-structural elements during and after low and moderate seismic events, contributing to a better interpretation of data provided by SHM systems. Regarding the paper contents, after a brief description of the laboratory mock-up, the whole experimental campaign is widely described in Section 2. Section 3 is devoted to the quasi-static tests used to produce damage to the infills, while Section 4 addresses results of dynamic tests performed on the structure; tests have the peculiarity of inducing excitation of increasing amplitude on the mock-up. Finally, a comprehensive comparison of results is given in Section 5, aiming to correlate the outcomes of different tests and to provide information for interpreting data from SHM systems, which are expected to register the structural response before, during and after seismic events.

2 Description of the experimental campaign

The tested laboratory mock-up is an infilled steel-concrete composite structure with two-bay moment resisting frames in the longitudinal direction and one-bay braced frame in the transverse one (Figure 1a). In the latter direction, two X-braces at the edge spans are mounted to entrust transverse forces. The mock-up is 8.40 m long, 2.80 m wide and 3.00 m high. The concrete slab is 0.12 m thick, casted on a collaborating steel sheet and connected to the steel frame with Nelson studs. Columns are fixed to the laboratory strong floor through post-tensioned anchor bolts. Concrete blocks are placed over the slab to simulate the mass of permanent and live loads. The infill masonry walls (W1 and W2) fill only one of the two longitudinal bays and are built with hollow clay bricks with bed and head mortar joints having thickness of about 1-1.5 cm (Figure 1b). A thin gypsum plaster layer, with thickness of about 0.7 cm, is placed over both sides of each wall. A more detailed description of the mock-up can be found in [35].

The mock-up was equipped with the instrumentation illustrated in Figure 2 in order to measure its response when subjected to quasi-static and dynamic tests. A double action actuator was mounted on one side of the frame in order to apply a non-eccentric longitudinal force at the level of the concrete slab. Three linear variable displacement transducers

(DT1, DT2 and DT3) were mounted on the opposite side of the actuator (Figure 2) and connected to the mock-up slab in order to measure the longitudinal displacement of the slab with respect to an external fixed system. Six uniaxial piezoelectric accelerometers were positioned over the concrete slab, three measuring in the transverse direction (AC1, AC2, AC3) and three in the longitudinal one (AC4, AC5, AC6), in order to in-depth investigate the mock-up dynamics and to obtain refined mode shapes. It is worth specifying that when dynamic tests were performed the actuator was always detached from the tested structure to avoid any interactions with the loading system.

Several types of tests were performed and a summary of the overall experimental campaign is reported in Table 1. At first, the bare (i.e., without infills) mock-up was investigated performing an Ambient Vibration Test (AVT) and several Impact Load Tests (ILTs). The former consists in measuring the structure accelerations produced by the ambient excitation, namely microtremors due to the surrounding environment, while the latter foresee the excitation of the structure through instrumented hammer blows and the recording of both impacts and produced accelerations. The hammer blows were provided in two slab corners (I1 and I2 in Figure 2) in order to excite both translational and rotational vibration modes. Results are used to identify the dynamics of the bare mock-up. Furthermore, Snap-Back Tests (SBTs) were performed, by pushing the mock-up in the longitudinal direction up to a predetermined displacement, and then by releasing it suddenly. Finally, Forced Vibration Tests (FVTs) were done as well, imposing a harmonic longitudinal displacement equal to ±4.0 mm with frequency ranging from 0.5 to 4.5 Hz. The investigated frequency range includes the resonance frequency of the bare mock-up longitudinal vibration mode, as it will be shown in the sequel. The above set of experimental tests is aimed to completely identify the linear behaviour of the bare mock-up.

After that, the two infill masonry walls were built and plastered. An AVT and several ILTs were repeated on the infilled mock-up to investigate changes on the mock-up dynamics due to the infill presence. At this stage the structure and the infills were undamaged. Successively, the frame was subjected to quasi-static displacements performing controlled Cyclic Load Tests (CLTs), each of them consisting in three reversed load cycles with the same displacement amplitude. CLTs were repeated twenty-five times, starting from an actuator longitudinal Stroke (S) of 1.0 mm and increasing it at each step, up to S = 13.0 mm. It is worth mentioning that the stroke of the actuator did not perfectly match the frame displacement measured through transducers DT#, because of the deformability of the steel elements used to physically connect the actuator to the frame (bolted stell plates). For this reason, Table 1 reports both the actuator strokes (S) and the actual longitudinal drift (d, calculated based on DT# measurements in push direction) obtained during each CLT. However, it is herein introduced that this issue does not affects the overall conclusions of the presented research. During CLTs, infills were progressively damaged due to the increasing In-Plane (IP) displacements which simulated an earthquake damage scenario, but the frame always remained in elastic phase. Between each CLT, ILTs and SBTs were performed as well. The latter were done by pushing the mock-up up to the same displacement amplitude reached in the previously performed CLT, in order to prevent the infill damage to progress. Finally, at the end of the CLT series, one more CLT was performed by pushing and pulling the mock-up exactly to a displacement equal to ± 12.0 mm, this time measured at transducers DT# (S = +14.0/-16.5 mm or d = ± 4‰); the latter test was performed to obtain a damage scenario on infills attributable to a symmetric IP load condition both in pull and in push direction. After the last CLT, an AVT and ILTs on the mock-up were performed to evaluate the residual modal properties, associated to a condition of completely damaged infills and elastic structure. According to the design of the steel frame, which foresees the elements yielding at a displacement of 15 mm [36], the absence of structural damage is expected; this was verified by the absence of visible steel frame damage. In addition, the elastic behaviour of the frame is also verified by results of numerical analyses performed on an available mock-up numerical model. More details about the numerical model and the analyses can be found in [36].

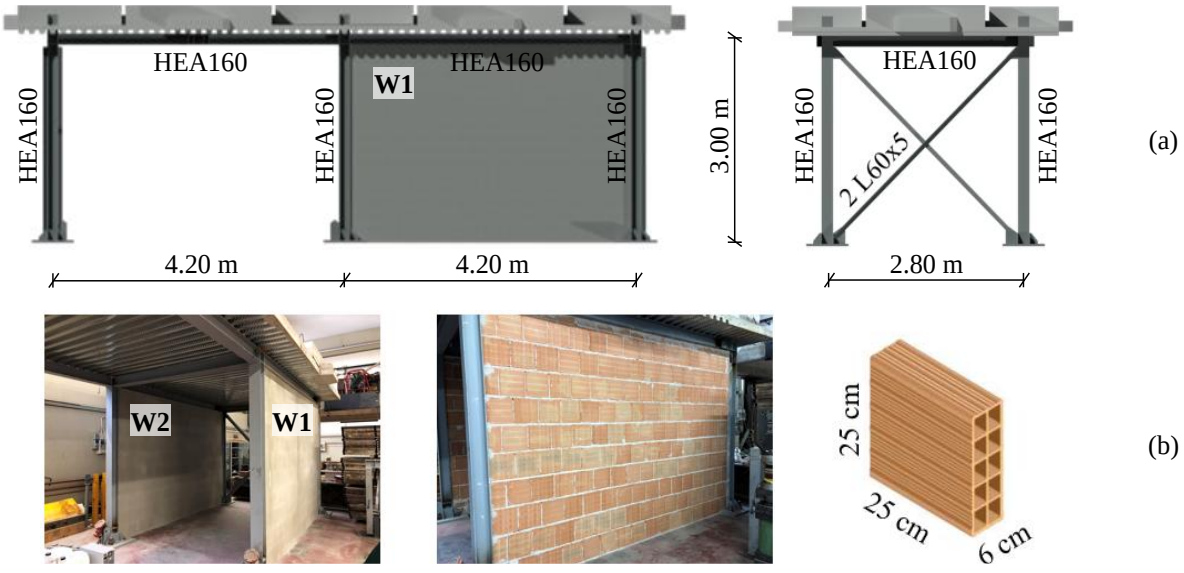

Figure 1. Laboratory mock-up: (a) longitudinal and transverse schemes, (b) infill masonry walls.

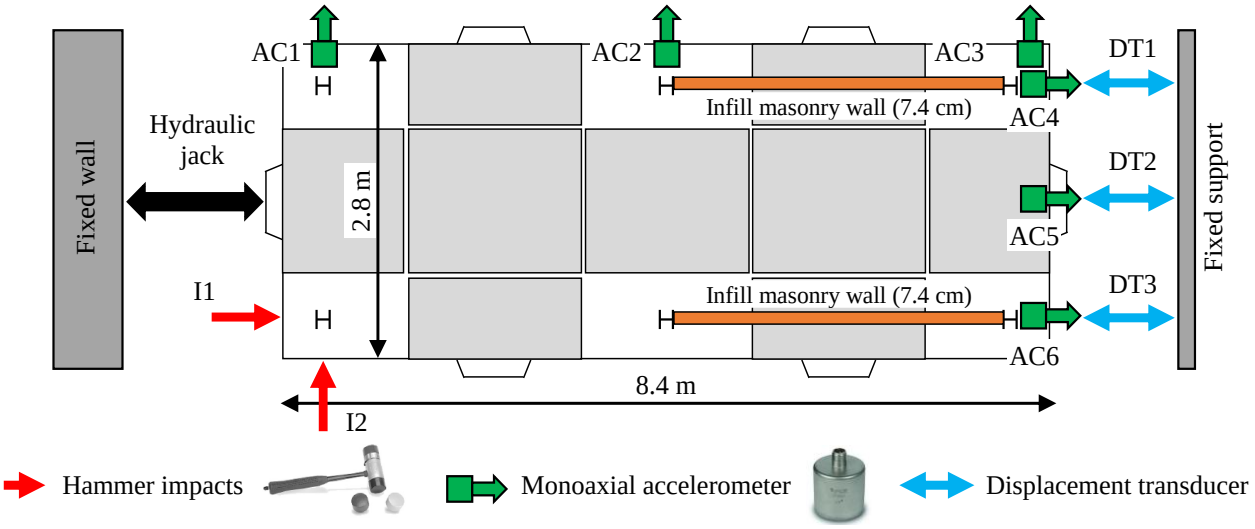

Figure 2. Instrumentation adopted for quasi-static and dynamic tests.

Table 1. Summary of the experimental campaign.

Mock-up description	Test sequence	Actuator longitudinal stroke *S* [mm]	Actual longitudinal drift *d* [‰]
Bare frame	AVT	---	---
	ILTs	---	---
	SBTs	2.0 – 4.0 – 6.0 8.0 – 10.0	0.44 – 1.17 – 1.78 2.45 – 3.12
	FVTs	±4.0 (from 0.5 to 4.5 Hz)	1.17 (from 0.5 to 4.5 Hz)
Infilled frame (no damage)	AVT	---	---
	ILTs	---	---
	CLTs		
Infilled frame (yes damage)	ILTs	from 1.0 to 13.0	from 0.10 to 3.90
	SBTs		
	CLT	+14.0/-16.5	±4.00
	AVT	---	---
	ILTs	---	---

3 Damage of infills due to quasi-static cyclic loads

As previously stated, CLTs are performed with the purpose of producing damage to infills simulating an earthquake damage scenario. Indeed, during quasi-static CLTs, infills progressively undergo damage due to the imposed increasing longitudinal displacements of the mock-up that produced forces correlated to the IP stiffness and strength of the infill masonry walls. For the structure at hand, the ultimate imposed interstorey drift is close to that producing the structure yielding, so that the investigation of the infill behaviour beyond a displacement of ±12 mm was not possible.

Crack patterns on infills are surveyed during the whole CLT campaign and the most significant ones for the evaluation of the damage evolution on infills are illustrated in Figure 3. Both infills exhibited no visible cracks up to an actuator stroke minor than about 5.0 mm (real drift around 0.90‰), then shallow and narrow diagonal cracks occurred on the top corners. For a stroke equal to 6.5 mm (real drift of 1.39‰), a horizontal crack around the mid height of W1 panel occurred along a bed joint, whereas a similar crack appeared in W2 at a stroke equal to 7.5 mm (real drift of 1.93‰). By increasing the actuator stroke, stair-stepped cracks begun to form and to get longer in both walls. At the end of CLTs (actuator stroke of 13.0 mm and real drift of 3.90‰) both walls exhibited a similar shear failure mechanism and were completely cracked.

The mock-up hysteretic cycles obtained from the experimental tests are depicted in Figure 4, together with their backbone curves. The latter show sudden drops in correspondence of an actuator stroke between 6.0 mm and 8.0 mm in push and pull directions; this sharp decrease is due to an important damage of both infills that leads to a reduction of both the IP stiffness and strength of the walls. However, the IP strength of infills kept increasing after this drop, while the secant stiffness (i.e., the equivalent stiffness associated to the maximum displacement achieved during a step) continued to reduce,

tending to the static stiffness of the bare mock-up ($k_{st,b}$); the latter, represented with dashed blue lines in Figure 4, is calculated based on the ramp of the displacement-force graphs obtained from SBTs on the bare frame, which is characterised by an almost linear behaviour. The analysis of cycles obtained for different strokes highlights a peculiar trend of the shear force-displacement relationships that is due to the progressive damage of infills and to the evolution of the resisting mechanisms of the non-structural elements with respect to horizontal loads. Indeed, as also demonstrated by the crack patterns previously discussed, the infill resistant mechanism to lateral forces is firstly governed by the shear response of the wall panel as a whole, which leads to the opening of horizontal cracks on the upper side of the walls, whereas, for higher actuator strokes, a strut mechanism on infills activated, leading to the opening of diagonal stair-stepped cracks.

The secant stiffness is calculated based on the first and third load cycle measurements for each stroke. The obtained values are plotted in Figure 5 (data from the first and the third load cycles are separately considered, plotted with blue and red lines, respectively), differentiating for push and pull directions. With reference to the secant stiffness evaluated from the first cycle (blue lines), it can be observed an initial longitudinal stiffness increase, probably because a certain level of displacement is necessary to activate the infill resisting mechanisms; then, after reaching the peak, a decrease is observed, and a sudden drop is well visible for strokes ranging between 6.0 and 8.0 mm (real drifts varying from 1.17‰ and 2.09‰). Finally, an almost constant decrease is noticeably up to the end due to the degradation of the final resisting mechanisms (essentially constituted by the frictions forces developing between cracks). The last stiffness values, although much lower than those relevant to the undamaged infills, are higher than the static stiffness relevant to the bare mock-up, demonstrating that the damaged walls, which have suffered almost 4‰ of interstorey drifts, still contribute to the longitudinal stiffness of the structure. To obtain a further comparison, the maximum ($k_{s,max}$) and the final ($k_{s,end}$) secant stiffnesses, together with the static one relevant to the bare frame ($k_{st,b}$), are represented with dashed lines in Figure 4. The secant stiffness calculated from data of the third load cycle of each step are also shown in Figure 5 with red lines. For strokes below 2 - 2.5 mm, the blue and red lines are almost superimposed; then, when infills start to damage, little differences are observed, and the red curves are always below the blue ones because of the degradation of the resisting mechanism due to the increasing number of cycles. In the last part of the graph, the two lines are still almost superimposed, revealing that the number of cycles no longer contributes to the degradation of the resisting mechanism.

Finally, results of the +14.0/-16.5 mm (real drift of 4‰) CLT are considered and discussed. Observing the relevant crack patterns of Figure 3 it is evident that both infills experienced a further damage, with bricks spalling (yellow bricks) in both panels. The secant stiffness of the mock-up is calculated as well, and results are reported in Figure 5; the mock-up secant stiffness in the pull direction shows a more pronounced reduction, being greater the difference between the actuator stroke and the maximum real displacement registered by transducers with respect to the push direction.

4 Dynamic tests during the infill damage

Three types of dynamic tests were performed on the mock-up during the whole experimental campaign to investigate changes in its dynamics due to the progressive damage of the infill masonry walls, and to evaluate the possibility of capturing the effects of damage from the analysis of the system excited by inputs of different amplitude. Indeed, the three dynamic tests are characterised by different levels of input excitation; in detail, starting from AVTs, the level of excitation (in terms of acceleration, velocity and displacement amplitudes) sensibly increases, passing through ILTs up to SBTs. The main aim is to provide correlations between the dynamic parameters of the system and the damage level experienced by the infills, also depending on the level of excitation. In the sequel, a generalised use of the term damage for infills is adopted to identify a change in their response that is reflected in the dynamic behaviour of the mock-up. Thus, small changes of the system dynamic properties that cannot be associated with visible infill damage may be related to the formation of micro-crack patterns or the degradation of the infills restraints conditions at the infill-frame interface. On the contrary, large changes of the system properties are often related to a significant and highly visible damage of panels. However, both could adversely affect the current or future performance of the infills, and it is quite difficult to determine whether or not a given change would be dangerous for human safety since even small cracks or the degradation of the infill-frame interface can affect the infill Out-Of-Plane (OOP) stability.

Before addressing tests executed on the mock-up, a brief overview of their effectiveness for detecting the structural dynamic properties is discussed, with also reference to applications in real structural systems. AVTs are commonly adopted worldwide to identify the dynamic behaviour of structures [37-40] because they offer several advantages. Indeed, they do not require a bulky equipment to be adopted, can be performed in structures without activity interruptions, and the input, provided by the environment, is capable to excite the entire structure. AVTs are also usually adopted in SHM systems to control changes in the dynamic behaviour of structures over time. Obviously, the identified modal properties characterise the dynamic behaviour of a structure during its operating conditions, i.e., when it is subjected to very low level of excitations, mainly due to microtremors produced by the surrounding environment (wind, traffic, and anthropic activities).

For ILTs the input to the structure is constituted by impulses that, differently than before, can be measured. This test typology is commonly used to test elements or parts of complex structures, while is seldom adopted to test structures as a whole (e.g., buildings, bridges, etc.) since it would require a high amplitude input for the system excitation, which may cause possible local damage. Moreover, the bigger the structure to excite, the higher the level of input to provide, sometimes very difficult to find and/or to apply. Only in few cases (e.g., low- and mid-rise structures), this test typology was successfully adopted to test the entire building [41,42]. Usually, the input is provided by hammer blows that produce an

impulsive force and allow the element to freely vibrate, but sometimes also by vehicles impacts, as in case of bridges where trucks pass on an artificial bump placed on the deck. Commonly, the input level is sufficiently low to avoid a non-linear response, and the identified modal parameters still characterise the linear dynamics of the tested element.

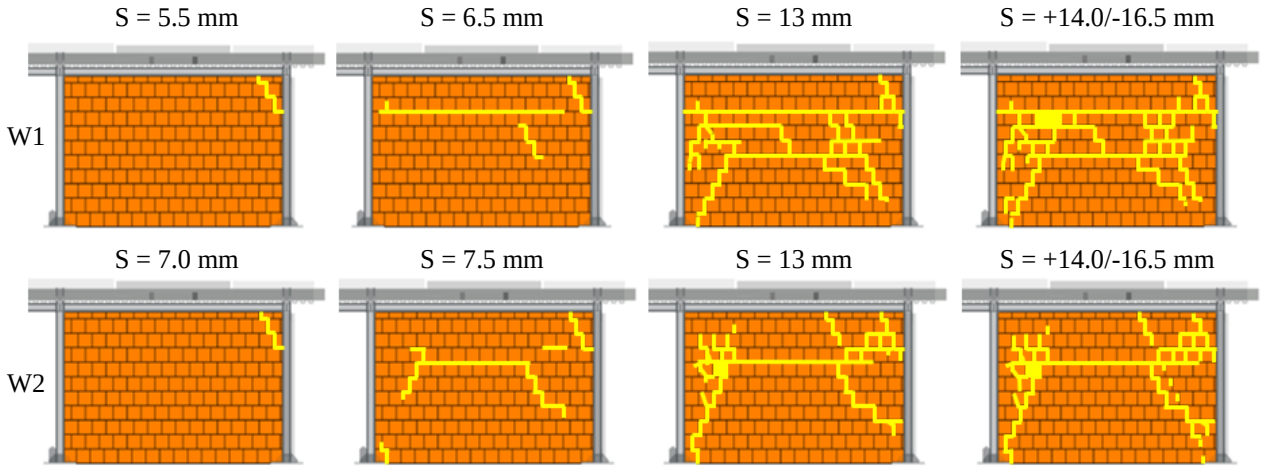

Figure 3. Crack patterns on infills surveyed during CLTs.

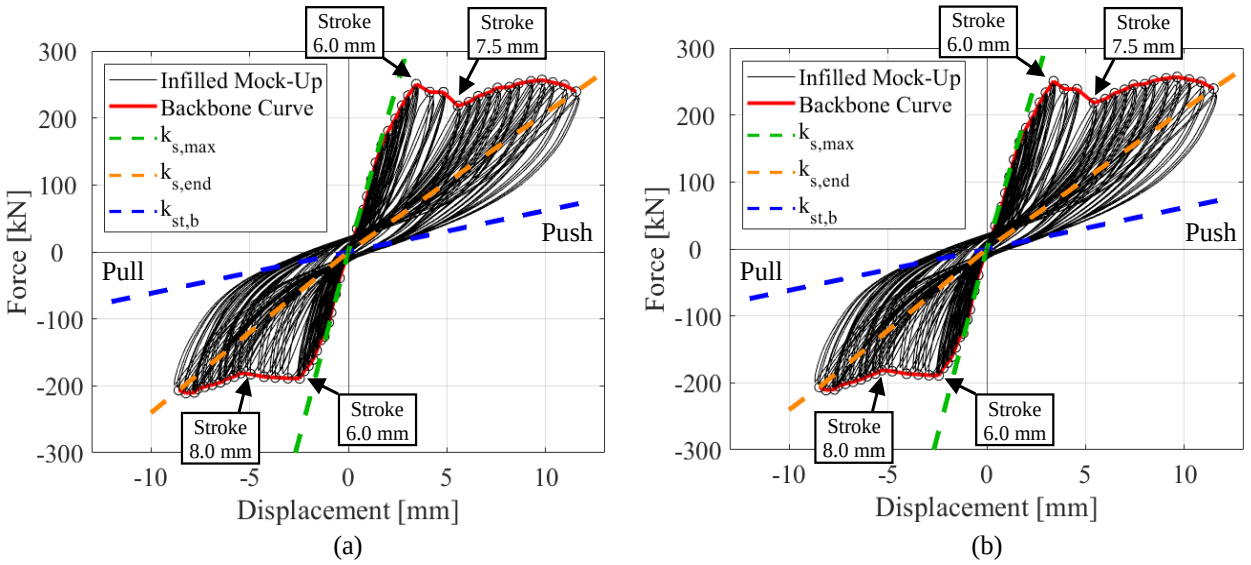

Figure 4. Mock-up hysteresis loops and backbone curves: (a) DT1, (b) DT3.

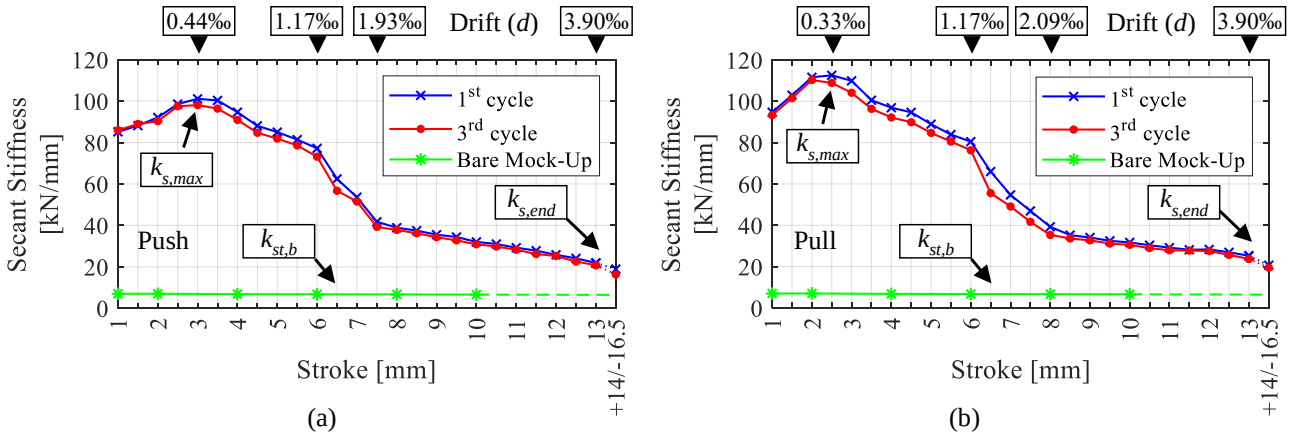

Figure 5. Mock-up longitudinal secant stiffness evolution: (a) push and (b) pull direction.

SBTs are seldom performed on real structures [43-45] since they require an important equipment to be constructed for the application of forces, which is often difficult to place in-situ, with high costs, and also because this kind of test should be carefully designed to avoid possible damage to structural or non-structural components. However, the excitation level provided to the structure is similar to that provided by low- and medium-intensity earthquakes, which can occur during the life of buildings in earthquake prone areas. In this sense, these tests are of particular interest because they allow the identification of the modal parameters of a structure under medium and high levels of excitations, as those provided by earthquakes. Usually, the latter differ from those identified from low amplitude vibrations (AVTs and ILTs) because friction forces (e.g., between structural and non-structural elements or existing cracks) can be overcome, making it possible to study effects due to the non-linear and non-stationary behaviour of the structure.

Despite applications of ILTs and SBTs can be found in the literature, these tests are used in the present research to excite the mock-up at different level of excitation in order to investigate correlations between the dynamic parameters of the whole system and the damage level experienced by the infills, depending on the level of excitation. Such as an example, the system response to SBTs can be compared to that induced by earthquake excitations of low and moderate intensities, and the building dynamics can be identified adopting suitable techniques (e.g., [9]) able to take into account the frequency content of the excitation and the time-variant nature of the response. On the other hand, the system response due to ILTs may be similar to that registered during a seismic swarm, while the response during AVTs is typical for the structural system subjected to ambient excitation.

The test output (accelerations or velocities) is commonly measured though sensors distributed throughout the investigated building. Sensors can be deployed during the measurement or can be permanently installed on the building to constitute a SHM system. The number and location depends on the test purposes: in case of a comprehensive dynamic identification (which includes the identification of mode shapes and possible damage localization applications), a significant number of sensors may be required to avoid the spatial aliasing and to achieve very detailed modal deflections. However, a dynamic monitoring system able of tracing frequency and damping ratio evolutions over time can be constituted by a reduced number of sensors (e.g., three accelerometers located at the roof level). In both cases, instrumentation is light, of small dimension, and tests can be performed without interrupting the building functionality.

In the sequel, the dynamic tests performed on the mock-up are described, and the main results are discussed. For each test typology, the input excitation level experienced by the mock-up is declared in order to correlate the obtained results with the relevant excitation sources.

4.1 Ambient vibration tests

AVTs were performed in three key phases of the experimental campaign, i.e., on the bare mock-up and on the infilled one, before and after the infill complete damage. The three tests were conducted in the same manner: ambient vibrations were recorded by the six accelerometers placed over the slab for a time length of about 20 minutes, adopting a sampling frequency of 2048 Hz. In a second phase, recorded data were inspected, corrected from spurious trends, filtered, and finally down sampled to make faster the subsequent analysis. As an example, in Figure 6 the accelerations recorded by AC5 during the three tests are reported. It can be noted that accelerations are characterized by similar and very low level of amplitudes, ranging between 10^{-5} and 10^{-4} g. To quantify the amplitude level, it is convenient to refer to the root mean square of the acceleration amplitudes. Again, for the AC5 records, the root mean square values are respectively 2.26, 3.23 and $3.03 \cdot 10^{-5}$ g for the bare, the infilled and the infilled damaged mock-up, respectively.

The mock-up modal parameters are identified based on the measured accelerations and using the Covariance-driven Stochastic Subspace Identification (SSI-COV) [46] output-only technique. For all the performed AVTs, three structural vibration modes are easily identified, namely the mock-up first two translational modes (longitudinal and transverse) and the rotational one. The relevant frequency values and damping ratios are listed in Table 2. As can be observed, the presence of infills (undamaged) sensibly increases (of about 6 times) the frequency of the longitudinal vibration mode with respect to the bare frame, demonstrating an important increasing of the mock-up longitudinal stiffness; also, the rotational mode increases (of about 15%) since the walls, due to their plan layout, contribute to the torsional stiffness of the mock-up. In any case, the latter contribution is limited because the walls are close to each other. On the contrary, as expected, the frequency of the transverse mode is slightly influenced by infills since their OOP stiffness does not sensibly increase the overall transverse stiffness of the mock-up. Moreover, the little decrease of the transverse mode frequency between the bare and the infilled mock-up (in absence of damage) is probably due to the mass increase, which mostly affects the dynamic behaviour of the structure rather than the transverse stiffness increment. The negligible contribution of the infills to the mock-up transverse stiffness is also confirmed by the frequency reduction observed between the undamaged and damaged condition (about 1.3%), which is extremely smaller than the reduction observed for the longitudinal (and also for the rotational) frequency. The infill damage clearly determines the reduction of all frequencies, especially that of the longitudinal mode, which reduces of about 38%. In any case, both the longitudinal and rotational vibration mode frequencies of the damaged system are higher than the corresponding ones of the bare frame; hence, despite heavily damaged, infills still contribute to increase the mock-up stiffness, as also observed from CLT results.

As for damping ratios, a slight increase is observed for the infilled mock-up with respect to the bare one, probably due to the higher dissipative potential of the infills with respect to the steel members. However, the reduction for the damaged system is less intuitive even if it should be observed that the system vibrations due to ambient excitations have a very low amplitude, so that dissipative mechanisms are difficult to be activated. However, all values are below 1%,

demonstrating that the structural damping is always very low. This suggest that, for the structural system at hand, AVTs are not adequate to capture the dissipative capabilities of the damaged system because the latter are essentially due to friction phenomena occurring within the damaged infills that cannot be activated by low amplitude vibrations.

Figure 7 depicts the mode shapes identified from the three performed tests, while in Figure 8 the Modal Assurance Criterion (MAC) indexes are reported. The latter are calculated between the same vibration mode shapes relevant to two consequent tests and provide an indication of how the mode shapes are similar to each other: the closer the index to one (black box), the more the mode shapes are similar. Observing Figure 8 it is possible to state that the mode shapes remain almost always the same, both after the infill construction and after the infill damage, and also the MAC indexes are very close to one. Only the first mode shape (relevant to the longitudinal mode) changes a bit after the infill construction, as can be also noted from the mode shapes represented in Figure 7, where the longitudinal mode relevant to the undamaged infills is slightly coupled with the rotation, probably due to the non-perfect symmetry of the two walls.

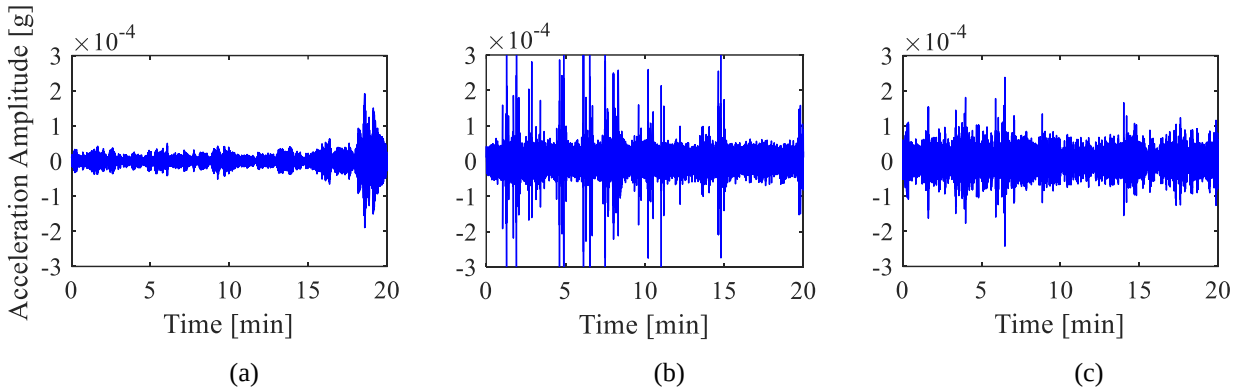

Figure 6. Accelerations recorded during AVTs: (a) bare mock-up, (b) mock-up with undamaged infills, (c) mock-up with damaged infills.

Table 2. Mock-up modal parameters identified from AVTs.

Mode	Mode type	Bare mock-up	Mock-up with undamaged infills	Mock-up with damaged infills
		Frequency [Hz]		
1st	Longitudinal	2.95	17.69	10.86
2nd	Transverse	8.42	8.37	8.26
3rd	Rotational	11.62	13.39	12.35
		Damping ratio [%]		
1st	Longitudinal	0.32	0.98	0.52
2nd	Transverse	0.55	0.67	0.58
3rd	Rotational	0.24	0.47	0.35

	Bare mock-up	Mock-up with undamaged infills	Mock-up with damaged infills
Longitudinal Mode	2.95 Hz	17.69 Hz	10.86 Hz
Transverse Mode	8.42 Hz	8.37 Hz	8.26 Hz
Rotational Mode	11.62 Hz	13.39 Hz	12.35 Hz

Figure 7. Mode shapes identified from AVTs.

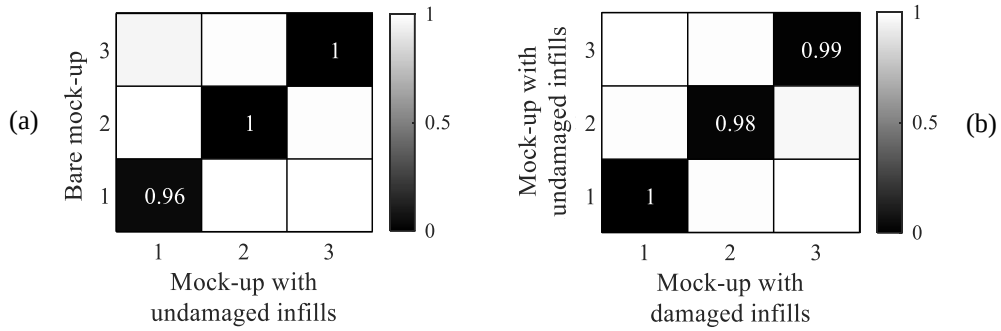

Figure 8. MAC indexes between the identified mode shapes: (a) bare mock-up *vs* mock-up with undamaged infills, (b) mock-up with undamaged infills *vs* mock-up with damaged infills.

4.2 Impact load tests

ILTs were performed on the mock-up to evaluate possible changes in the identification of its global dynamic behaviour, expressed in terms of modal parameters, as a consequence of a higher excitation level. As previously stated, this test methodology is usually not suitable for testing whole structures; however, the limited dimensions of the mock-up made it possible to excite the whole structure providing hammer blows manually through an instrumented hammer of about 1 kg. Tests were performed in all phases of the experimentation: on the bare frame, just after the infill construction, during the infill damage (after each CLT), and finally, at the end of the experimental campaign. The test protocol foresaw the application of hammer blows at the slab corners (Figure 2a) and the recording of input and output accelerations measured by the accelerometers placed over the slab (the same adopted for AVTs). For each test, at least three hammer blows were provided for each impact point, so as to obtain a reliable data set; for each blow, 50 s long signals (both the impulse and accelerations) were recorded to achieve a good frequency resolution on the subsequent outputs. Both input (hammer blows) and output (accelerations) were recorded adopting a sampling frequency of 2048 Hz. As an example, in Figure 9 the impacts provided in I1 and the relevant accelerations recorded by AC5 are reported, considering tests on the bare and on the infilled frame. As can be seen, the highest accelerations reached in correspondence of the impact applications are of the order of $1 \div 2 \cdot 10^{-2}$ g, then they rapidly decrease. Obviously, the acceleration amplitude depends on the impact force given to the structure, but for all the performed ILTs very similar impacts were provided to the structure, and accelerations always show this order of amplitude.

The modal parameters of the mock-up are identified adopting the Numerical algorithm for Subspace State Space System IDentification (N4SID) [47], which is an input-output identification methodology working in time domain. Indeed, differently from AVTs, in this case also the input provided to the structure (hammer blows) was measured thanks to the instrumented hammer. The methodology allows the identification of the resonant frequency, damping ratio and mode shape of each vibration mode. In Figure 10a the resonant frequencies identified during the experimental campaign are reported. As can be observed, after the infill construction ("Infilled" entry in the graph) the mock-up resonant frequencies relevant to the longitudinal and rotational modes sensibly increase with respect to the bare frame, especially the first one, while that relevant to the transverse mode remains almost the same. Then, during CLTs (from 1.0 to 13.0 mm longitudinal strokes), different frequency trends can be recognised: frequencies relevant to the transverse mode remain almost constant, those relevant to the rotational mode slightly decrease, while those relevant to the longitudinal mode show an evident decrease, especially during the last CLTs. Above results are consistent with observations previously made, where the contribution of the infills on the longitudinal and transverse stiffness of the mock-up has been addressed. At the end of the experimental campaign (after the +14.0/-16.5 mm CLT) the frequency of the longitudinal mode drops below that relevant to the rotational mode. The pronounced decreasing trend in the longitudinal mode frequency demonstrates a mock-up stiffness reduction, particularly in the longitudinal direction, due to the infill damage. This trend seems to be rather linear, except at the end, and in correspondence of longitudinal strokes equal to 5.5 and 6.0 mm, approximately the same previously discussed for which infills show the first important cracks.

Identified damping ratios are plotted in Figure 10b; in this case, no evident trends are visible. Nonetheless, it is worth observing that damping of the transverse and torsional modes are around 1% (values that are fully compliant with those obtained from the AVTs) while damping relevant to the longitudinal mode presents a higher variability, with values varying between 1 and 2%. This higher variability can be reasonable justified by recognising that the infill damage mainly affects the mock-up response in that direction, even if values are still low.

As before, mode shapes are compared using MAC indexes, and results are reported in Figure 11. Each mode shape is compared with the corresponding one at the previous step of the experimental campaign. For what concerns the longitudinal mode, the highest variations in the mode shapes are observed at the beginning of the CLTs (between strokes of 3.0 and 3.5 mm) and at the end of the experimental campaign (for strokes between 11.0 and +14.0/-16.5 mm), even if these variations are almost negligible, due to the relative high values of MAC indexes (never lower than 0.88). The changes found at the beginning are probably uncorrelated with the infill cracking, while changes found at the end of the experimentation are probably attributable to the development and enlargement of infill cracks. Similar considerations stem

from the observation of MAC indexes of the rotational mode, which never go below 0.84. Contrarily, the translational mode shapes remain almost always unchanged, with MAC values almost always equal to 1.0.

Summarising, for what concerns ILT outcomes, the infill damage produces high variations in terms of frequency values, but not in terms of damping ratios and mode shapes. It is worth repeating once again that these modal parameters are determined through low-amplitude dynamic tests.

4.3 Snap-back tests

SBTs were performed on both bare and infilled mock-up with the aim of identifying its dynamic behaviour in the longitudinal direction in case of greater excitation amplitudes. Indeed, the instantaneous release of the actuator (obtained by programming a sudden return of the cylinder) produced oscillations of the mock-up in the longitudinal direction that were measured through the accelerometers placed over the slab (AC4, AC5, AC6 in Figure 2). Obviously, these tests do not allow the investigation of the behaviour in the transverse direction; however, as observed in the previous sections, the longitudinal direction is clearly the one of greater interest in this study because it involves the IP stiffness and strength of infills.

Figure 12 shows the accelerations recorded from sensor AC5 during the tests with 2.0 mm of stroke, both for bare and infilled structure. It can be noted that the acceleration amplitudes experienced by the bare mock-up are much lower than those of the infilled one, due to the much higher stiffness of the latter. Moreover, SBTs on the bare mock-up produced a very high number of cycles, contrarily to what happened to the infilled structure, where the higher structural damping quickly dampens the oscillations. During the SBTs performed on the infilled mock-up, the acceleration amplitudes ranged from around 0.05 g (for the stroke of 1.0 mm) to 0.5 g (for the stroke equal to 13.0 mm).

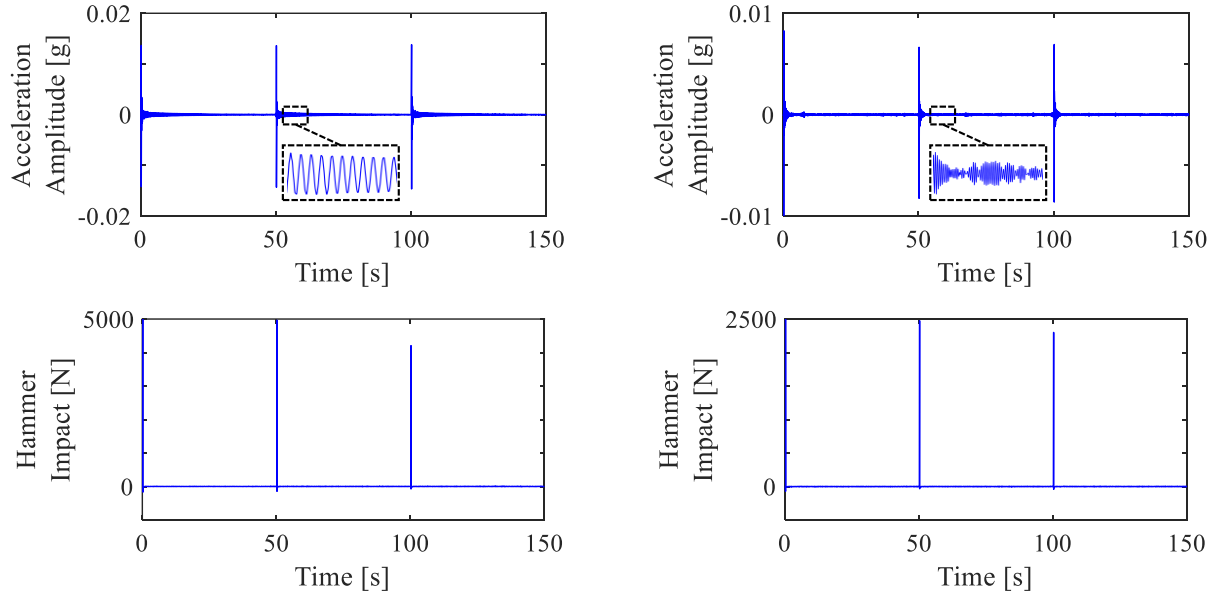

Figure 9. Examples of acceleration and impact records: (a) bare and (b) infilled mock-up.

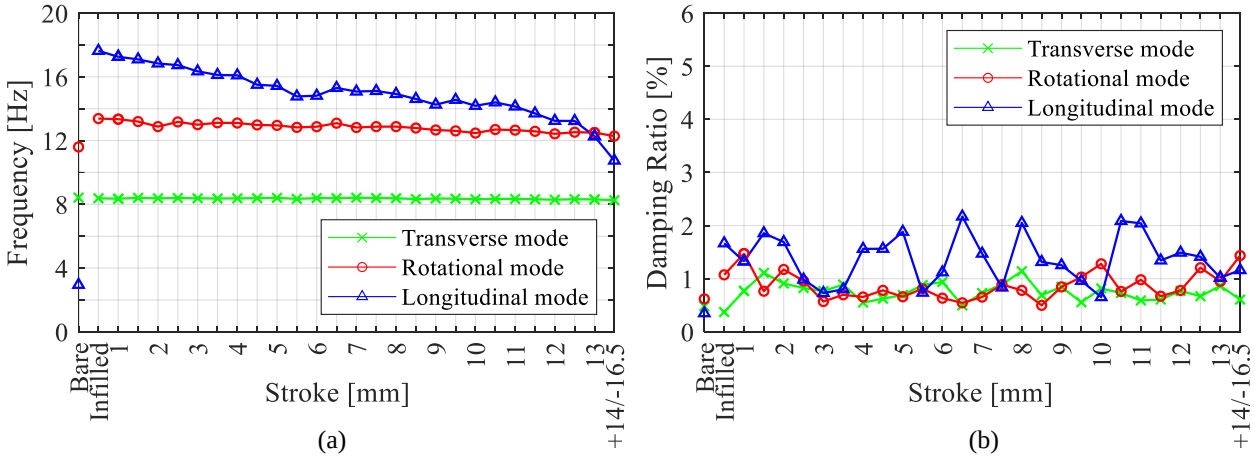

Figure 10. Mock-up modal parameters identified from ILTs: (a) resonant frequencies, (b) damping ratios.

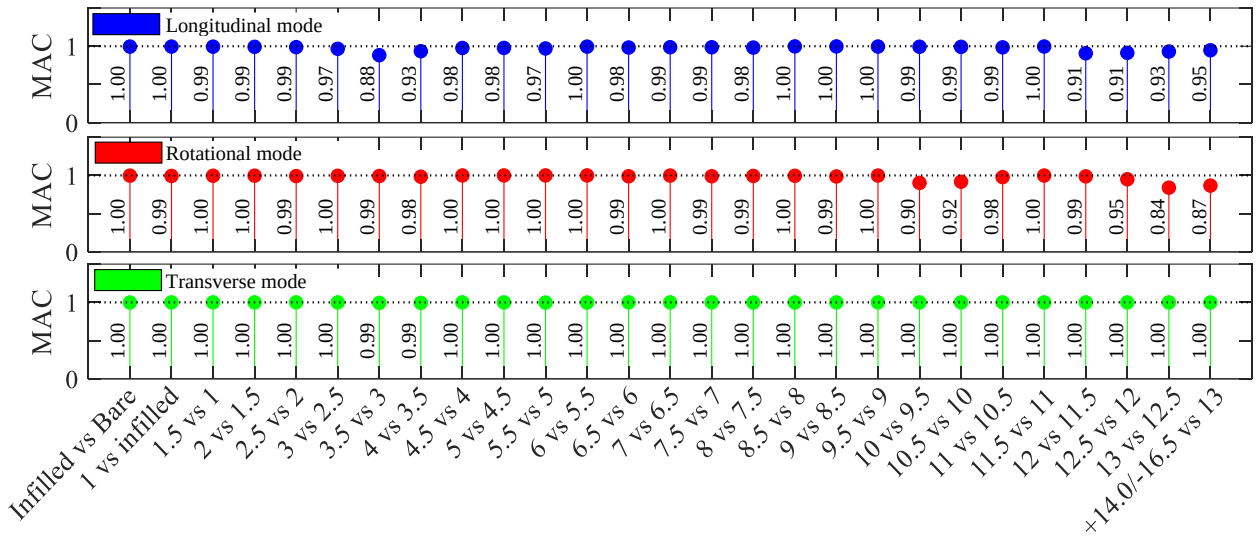

Figure 11. MAC indexes between mode shapes identified from ILTs.

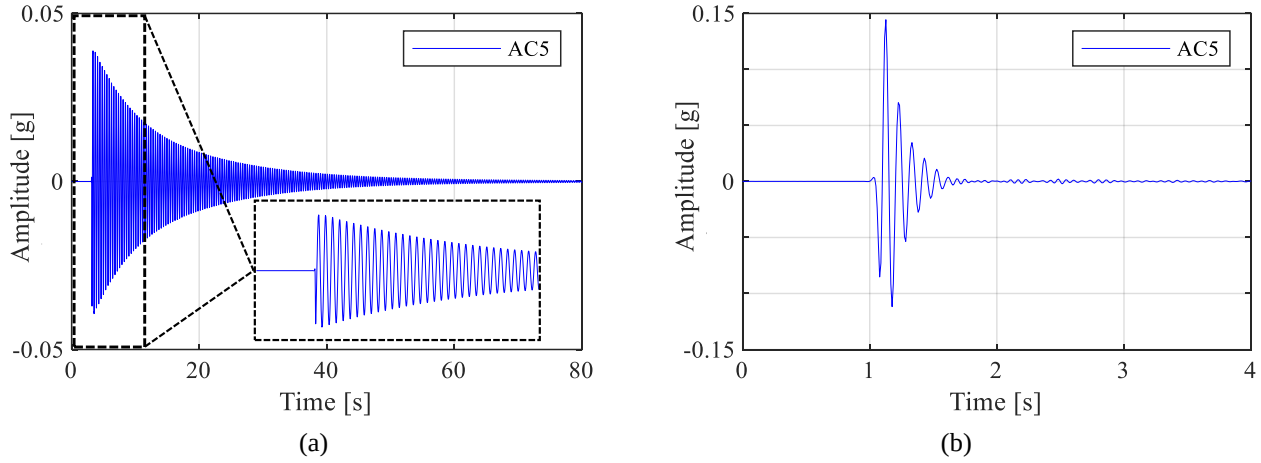

Figure 12. Accelerations recorded by AC5 during the 2.0 mm SBT: (a) bare and (b) infilled mock-up.

From the analysis of the free vibration part of the recorded accelerometric signals, it is possible to determine the resonant frequency of the mock-up relevant to the longitudinal vibration mode. The peak-picking method is adopted to individuate the maximum positive (push direction) peaks, and the time required to complete one cycle of vibration (peak-to-peak) is estimated. The resonant frequency is then calculated as the inverse of that period. Obviously, many frequency values are estimated for the bare mock-up (whose response is characterised by many peaks), while only few values can be obtained for the infilled mock-up; in detail, only the first two frequency values have been calculated because they always resulted clearly identifiable. The frequency values calculated with the peak-picking method and relevant to the mock-up longitudinal vibration mode are reported in Figure 13a as a function of the actuator stroke. As can be observed, a minor number of tests were performed for the bare frame (represented with black asterisks), and the estimated frequency values are almost constant and around 2.70 Hz. As already observed, for the infilled frame the frequencies are sensibly higher and depends on the stroke (and hence on the infills damage). For the first SBT performed at 1.0 mm stroke, the frequency value reach about 11.0 Hz, which is about four times greater than the frequency of the bare mock-up. Then, frequencies show an overall decrement as the imposed displacement (and the relevant infill damage) increases. Nevertheless, the frequency decrement is characterised by two rather evident trends: a first part (up to a stroke of 6.5 mm) with a pronounced decreasing trend, and a second part (from a stroke of 7.0 mm up to the end) with an attenuated decreasing trend. The change in the decay trend can be attributed to a change in the resisting mechanism of infills, as stated before. Decrements are due to the infill progressive damage to which a stiffness reduction in the longitudinal direction of the mock-up corresponds, as well as to the increasing of acceleration amplitudes. At the end of tests (stroke of 13.0 mm), the frequency of the infilled damaged mock-up is greater than that of the bare mock-up, as also previously observed from other tests, demonstrating the residual contribution of infills to the overall structural stiffness.

From the free vibration signals, the damping ratios of the mock-up longitudinal oscillation mode can be also computed. The latter are calculated adopting the logarithmic decrement method [48], which considers the natural logarithm of the ratio between two successive peaks of the accelerometric signal. The calculated damping ratios are reported in Figure

13b. In this case, some trends are clearly evident: from the beginning up to a stroke of 5.5 mm, the damping is almost constant with values around 10-15%, then it increases up to a stroke equal to 7.0 mm, due to the development of the main damage on infills, and finally it remains almost constant, with values around 15-25%.

Focusing on a single SBT, it is worth noting that the frequency of the longitudinal vibration mode exhibits a non-stationary evolution over time. This phenomenon is evident observing Figure 14, where Short Time Fourier Transforms (STFTs) of accelerations measured by accelerometers for three different actuator strokes (1.0, 7.0 and 13.0 mm), are depicted. In all cases it is possible to see a sharp decrease of frequency in correspondence of the beginning of oscillations, namely when the mock-up is suddenly released; then, the frequency tends to return to higher values. The frequency decrease is mainly due to the high level of oscillation amplitudes at the beginning of test, which activate non-linear mechanisms on infills, as frictions between the steel members and the infills, and frictions between cracks, resulting in a high deformability of the mock-up. After that, the oscillation amplitudes sensibly decrease, and the frequency tends to increase. Above phenomena have been also treated in other scientific works [49,50].

The lower frequency value reached for each SBT (f_{STFT-l}) is determined analysing the STFTs, together with a rough estimation of the higher frequency values to which the mock-up tends after the oscillation ($f_{STFT,h}$). Indeed, the latter frequency is quite difficult to be estimated from STFTs since the free vibration parts of the accelerometric signals present a wide frequency band rather than an evident peak, as clear from Figure 14. The range of f_{STFT-l} and f_{STFT-h} at each SBT is reported in the candlestick graph of Figure 15, where it is evident that the trend of f_{STFT-l} is very similar to that reported in Figure 13a.

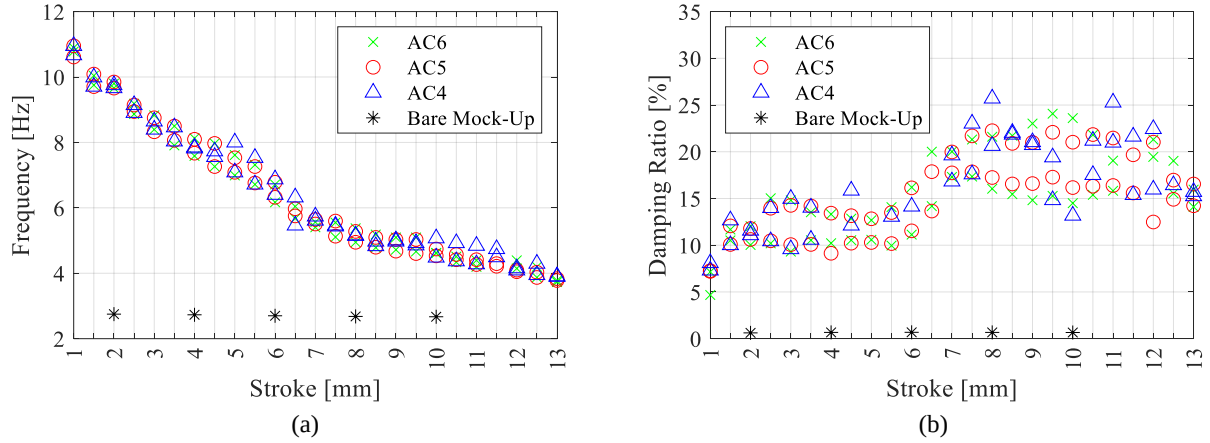

Figure 13. Modal parameters of the mock-up longitudinal vibration mode: (a) frequencies, (b) damping ratios.

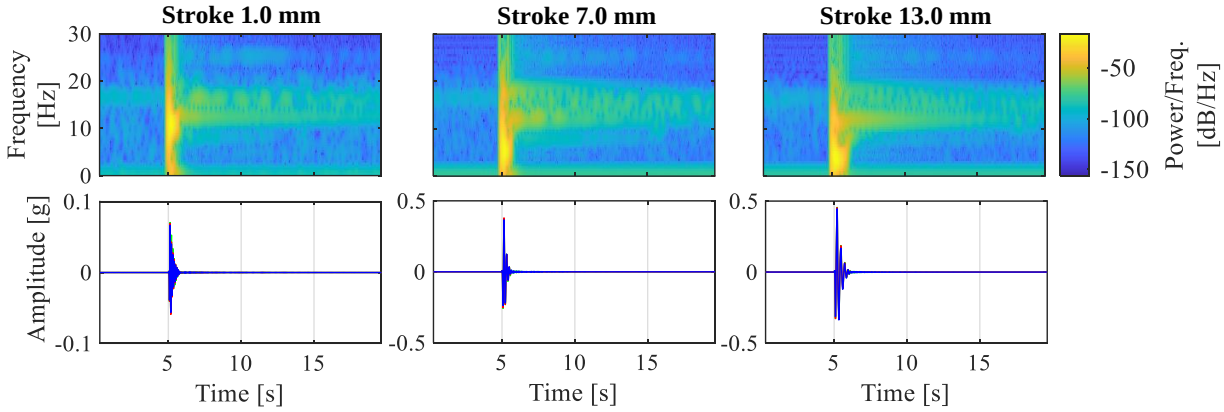

Figure 14. STFTs of the SBT accelerometric signals for strokes of 1.0, 7.0 and 13.0 mm.

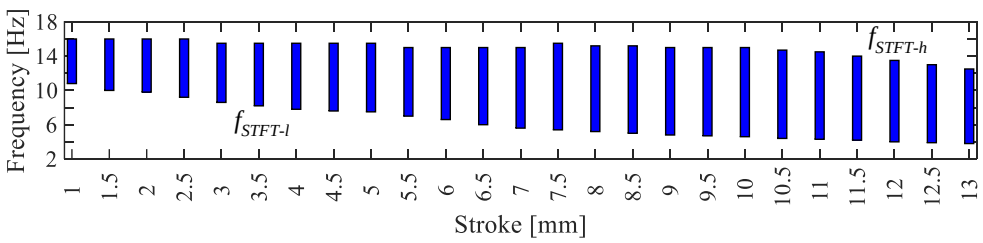

Figure 15. Range of frequency values estimated for each SBT from STFTs.

5 Comparison and discussion of test results

Results of tests performed on the mock-up during the infill progressive damage are analysed, compared, and discussed in this Section. Firstly, for the purpose of the results generalization, it should be remarked that the onset and the development of the infill damage strongly depends on both the material and geometrical properties of infills and the surrounding frame, as well as on the construction techniques and the type of stress state mobilized in the panel. The damage evolution observed on the tested infills is consistent with that observed in other real experimentations available in the literature [51,52], where masonry infills built in contact with the surrounding frame are tested under IP cycle loads. A collection and classification of the main failure mechanisms for masonry infilled frames can be found in [53,54]; in these works, five main causes of damage and failure are proposed: the failure of the surrounding frame, the shear sliding, the corner crushing, the diagonal compression, and the diagonal tension (cracking) of infills. In the presented case study, two of these damage causes are well recognised: firstly, the shear sliding occurred (for drifts around 1.4 and 2‰) producing horizontal cracks on mortar bed joints on both infills approximately at the centre of the panels; then, diagonal tension mechanisms activated up to the end of tests, which produced diagonal cracks mainly in correspondence of the bed and head mortar joints. The former damage is symptomatic of a strong frame coupled with weak mortar joints, while the latter of strong brick elements combined with weak joints. Moreover, the tested infills can be classified following the macro-classification approach proposed in [55], which consists in dividing the most common infill typologies built worldwide into five main classes as a function of several parameters, along with their thickness, stiffness, and strength. Following this classification, the tested infills are representative of the "weak" typology, which is characterised by thickness lower than 8 cm, elastic moduli (both vertical and horizontal) lower than 2000 MPa, and vertical and lateral strength lower than 2.02 and 1.18 MPa, respectively.

For a better understating of the infill response under IP loads, the boundary conditions of the infills, which are bounded by a steel frame, must be discussed as well. This aspect is very important since different infill constraints may lead to different structural and non-structural responses when subjected to horizontal cyclic (seismic) loads. This topic is discussed in many scientific and technical works [53,56,57]. As well known, due to the different lateral stiffness of the masonry infill panel and the surrounding frame (steel or RC elements), a disconnection between the panel and the frame is observed by increasing the displacement, except for two opposite corner zones, which are commonly defined as contact length. The entity of the contact length significantly affects the distribution of shear and moment in the surrounding frame, as well as the stress state within the infill panel [53]. For example, if the contact length is very short, the infill damage could be due to corner crushing of infills, namely crushing of the bricks near the beam-column joints due to high compression forces, but also to the failure of the surrounding frame with the development of plastic hinges or, in worst cases, to brittle shear failures.

By the analysis of the CLT results, the development of the infill damage is recognised in two different ways: by visual inspections and by tracing the hysteretic cycles of the system in terms of force-displacement curves; as shown, the latter approach is also suitable to evaluate the secant stiffness of the structure. By comparing the recognized crack patterns (Figure 3) with the hysteretic cycles (Figure 4), it is evident that the stiffness and strength of the structure (and hence of the infills) reduce at the formation of the first important horizontal cracks. However, the reduction is followed by a subsequent increment of strength, while the secant stiffness decreases up to the test end; this behaviour can be attributable to a change in the resisting mechanism of the damaged infills and it is probably due to the formation of the classical strut resisting mechanism after the opening of horizontal shear cracks. When infills are completely damaged, their contribution to the overall stiffness of the mock-up is low but not negligible since higher values of secant stiffness are observed for the completely damaged infills with respect to the bare frame. Presented data contribute to correlate the observed damage on infills with their residual strength and stiffness, which is a very important task for the safety assessment of building during visual inspections after earthquakes. For example, for the considered case study, the percentage variations of the secant stiffness and of the global strength (the latter expressed as the maximum horizontal force resisted by the infilled mock-up, evident from the backbone curve) due to the progressive damage of infills are reported in Table 3, and are correlated with the damage observed on both infills, and with the actual drifts to which the non-structural components were subjected. The percentage variations of each state are calculated with respect to the previous one and only refer to the push direction since the pull one provides very similar results. As can be seen, the formation of the horizontal cracks resulted in a strength reduction of 13% and a longitudinal secant stiffness reduction of 45%, while the formation of diagonal cracks is correlated to a slight strength increment (10%, probably due, as stated before, to the activation of different resisting mechanisms within the infill panel), and to a further stiffness decrement (55%). A critical analysis of results proposed in Table 3 can also support practitioners in decision-making procedures when they have to evaluate the healthy status and the useability of infilled structures stroked by earthquakes. This is a fundamental aspect, especially for buildings with public and strategic functions, for which an interruption of the activities may have catastrophic consequences in the emergency management, but also for private edifices; indeed, a temporary or permanent uninhabitability of houses can cause many displaced people with consequent discomfort and high costs for the whole community. As for the considered case study, for very small drifts (between 0.1 - 0.4‰), the degradation of the infill panel-frame interface and the formation of small and shallow cracks on the panel corners produced a low frequency decay and was associated to an increase of both strength and stiffness; hence, it is possible to assert that infills did not suffer a real damage and that the change in frequency is associated to a degradation of the boundary conditions that are necessary for the development of the panel resisting mechanism. On the contrary, for higher drifts, the formation of horizontal cracks (firstly) and of diagonal cracks (secondly) resulted in high stiffness decays

that lead to conclude that the infills are no longer in a safety condition for the building occupants. Indeed, even if the strength continued to increase, probably the stability against OOP action was compromised. However, the correlation of the stiffness decay with a safety condition of the panel must be based on a significantly larger set of experimental data, to cover a large variety of situations, infill typologies and boundary conditions. Thus, since visual inspections remain always the most easy and fast-to-perform tool to evaluate the health condition of a structure and of its non-structural components after earthquakes, it is of interest to correlate infill strength and stiffness values to their health conditions on the basis of in-situ infill crack patterns recognition. Results of the presented research provide some interesting data to this purpose.

In addition to CLTs, dynamic tests were also performed in order to investigate the possibility of identifying damage to non-structural components from the analysis of the system response subjected to different excitation amplitudes. In this Section, only results concerning the mock-up longitudinal vibration mode are considered since it represents the mode mostly affected by the infill damage occurrence. Obviously, in real buildings, where panels commonly fill all the perimetric frames, all the vibration modes, especially the first translational ones, are affected by the infills presence and damage.

At first, the resonant frequencies identified at each step of the CLT procedure are considered, and reported in Figure 16a. As can be noted, two different groups are well visible: the first one on the upper part of the graph refers to frequency values identified from AVTs and ILTs, together with those estimated from the free vibration part of the STFT graphs (STFT-h); the second one, placed on the bottom level, refers to frequencies identified through peak picking method starting from SBT measurements (Snap-Back Peak-Picking considering the 1st cycle, SB-PP-1st, and Snap-Back Peak-Picking considering the 2nd cycle, SB-PP-2nd), and frequencies estimated from STFT graphs in correspondence of the mock-up release during SBTs (STFT-l). These two frequency groups identify two test groups that are characterised by different level of amplitude excitations; in detail, the first one gathers frequencies identified from tests with low level of input excitation, while, for the second one, the level of excitation increases. The frequency interval between them demonstrates that longitudinal frequency is sensitive to oscillation amplitudes on which non-linear phenomena depends. Nevertheless, it is noteworthy to point out that a frequency decay is always visible, considering all performed test typologies, demonstrating a mock-up global stiffness decrease due to the progressive infill damage. Hence, it can be asserted that tracing frequency values is a useful tool to monitor the health status of a structure and to support the damage identification procedure. However, the observed frequency decay is almost linear, so that it cannot help to detect the specific phases of the experimental campaign (strokes and drifts) in which the main damage occurred. This is also evident by observing data of Table 3; indeed, focusing on the percentage variations calculated based on frequency values identified from low-amplitude tests, no evident variations are found in correspondence of the horizontal cracks formation (for which an almost constant frequency trend is evident). However, when infills are completely damaged (horizontal and diagonal cracks are occurred), the drop in frequency is very important (-30%). The same considerations stem from the analysis of high-amplitude frequency trends. It is interesting to observe that the drastic drop of longitudinal secant stiffness experienced by the mock-up for strokes between 6 and 8 mm (as visible in Figure 5) is not associated to an equally sharp decrease in longitudinal frequency. In fact, as previously observed, the frequency decays detected from low- and high-amplitude tests are almost linear. For low-amplitude tests this may be reasonably since the dynamic excitation provided to the mock-up is not so high to activate non-linear and dissipative mechanisms; as for high-amplitude tests (SBTs), the phenomenon may be justified by the fact that the non-linear mechanisms (e.g., due to frictions) are activated only for the few cycles characterised by the higher amplitudes, as can be seen from Figure 12b. It is worth pointing out that for real buildings a frequency decay should be detected for all vibration modes and, especially, for the first translational ones, which are those mainly influenced by the IP stiffening contribution of infills. Moreover, a non-uniform damage of infills (as well as of structural members) can also lead to changes on the dynamic response of a building, which means that both frequencies and mode shapes may vary. So, tracing the frequency decay together with controlling the mode shapes could allow the triggering of possible damage and, in some cases, also to locate it.

Figure 16b depicts damping ratios identified for the same tests previously discussed. Also in this case, damping ratios can be divided into two groups: the first one (in the bottom part of the graph) refers to damping ratios obtained from AVTs and ILTs, while the second one (upper part of the graph) refers to SBT measurements.

Table 3. Percentage [%] variation of mock-up longitudinal characteristics (for push direction) due to infill progressive damage and correlation with the observed infill damage.

Stroke [mm]	Drift [‰]	Infill states	Strength	Secant stiffness	Frequency (low-amplitude)	Frequency (high-amplitude)	Damping (high-amplitude)
0	0	Undamaged	---	---	---	---	---
1.0 to 3.0	0.10 to 0.40	Panel separation from the frame and activation of the initial resisting mechanism	+284	+17	-4	-20	+7
3.0 to 6.0	0.40 to 1.17	Diagonal cracks at the top corners	+88	-24	-8	-23	+10
6.0 to 7.5	1.17 to 1.93	Horizontal crack at approximately the mid-height of panels	-13	-45	+1	-18	+48
7.5 to end	1.93 to 4.00	Diagonal cracks and brick spalling	+10	-55	-30	-30	-5

The group on the bottom part of Figure 16b (AVTs and ILTs) does not show any visible trend; contrarily, the group on the upper part (SBTs) illustrates two evident trends: low damping values at the beginning followed by a noticeably increment (starting from a stroke of 5.5 mm) up to a value that remains almost constant till the end. Differently from frequencies, damping ratios identified from tests with a low excitation level are not useful to investigate dissipative capabilities of the damaged mock-up since no significant trends are recognised, so their use in a SMH monitoring is not meaningful. On the other hand, damping ratios identified from SBTs are capable to capture steps when the main damage to non-structural components occurs. This is also confirmed by observing data of Table 3, in which a high increasing in damping is observed when the horizontal cracks occurred in the infills (about +50%). The almost constant damping ratio after the horizontal and diagonal crack opening demonstrates that infills have developed a stable dissipative mechanism that is independent on the amplitude of oscillations. Summarizing, it can be asserted that the evolution of damping ratios can be suitably identified from recordings of SHM systems in case of low seismic events (or during the seismic swarm following a main shock). In other words, outcomes of this research relevant to SBTs can be correlated to those achievable from the analysis of acceleration (and/or velocity) records due to earthquakes, able to activate non-linear phenomena on the building.

Differences in longitudinal mode shapes are not taken into account because it has been highlighted in previous Sections that the longitudinal mode has always the same shape, as demonstrated from high MAC values obtained from different dynamic test typologies and at different CLTs. Moreover, it has been demonstrated ([58]) that the damage of structures subjected to seismic loading determines significant changes in frequency values and damping ratios, but small changes in modal displacements, if the damage is widespread in the structure.

Also, quasi-static tests (CLTs) and dynamic ones (AVTs, ILTs and SBTs) can be compared in terms of stiffness that characterises the mock-up longitudinal behaviour. Figure 17a reports hysteretic cycles obtained from DT1 measurements (those of DT3 provide a very similar graph) and secant stiffnesses calculated in crucial phases of the experimental campaign. It is worth remembering that these secant stiffnesses need to be considered as an equivalent stiffnesses for the mock-up, especially once it experienced a certain level of damage. The dynamic stiffnesses (k_d) are calculated starting from results of different tests and assuming that the mock-up behaves as a SDOF system in longitudinal direction, which is a reasonable hypothesis considering that the majority of mock-up mass is concentrated at the floor level. Thus, the simple formula providing the fundamental frequency of a SDOF systems can be adopted to get the system dynamic stiffness according to $k_d = 4\pi^2 f^2 m$, where m is the effective mass and f the natural frequency of the longitudinal vibration mode.

To compute the contribution of infills on the effective mass m, half height of walls is considered, as reported in Figure 17b, while the effective mass of the bare mock-up is determined exploiting results of FVTs. The latter are performed on the bare mock-up at different frequency excitations and for a stroke equal to ±4 mm (Table 1). From FVTs, the dynamic stiffness of the bare mock-up (i.e., the force necessary to produce a harmonic displacement of amplitude 4 mm) can be determined by dividing the output (displacement) by the input (force) evaluated at stationary conditions. The obtained absolute values of the dynamic stiffness as a function of the excitation source frequency, are shown with a black continuous line in Figure 17c. Instead, Figure 17d shows typical hysteretic cycles obtained from tests at steady conditions. By supposing the damping of the bare structure to be negligible, the dynamic stiffness of the SDOF system can be determined with the regression function $k_d = k_{st} - (2\pi f)^2 m$, and the contribution of the bare frame to the effective mass can be estimated by adopting the previous formula to interpolate experimental data once k_{st} is known. The latter term (k_{st}) is obtained from SBT results executed on the bare frame. At the end of these procedures, the effective mass of the bare mock-up is estimated equal to 24 t, and the relevant regression function is shown in Figure 17c with a dashed black line. Consequently, the total effective mass of the infilled mock-up is obtained adding the effective mass of the bare mock-up with that of the infills, obtaining m = 25 t. It is worth mentioning that the real value of the mass of each infill is evaluated during the wall demolition by weighting all waste materials.

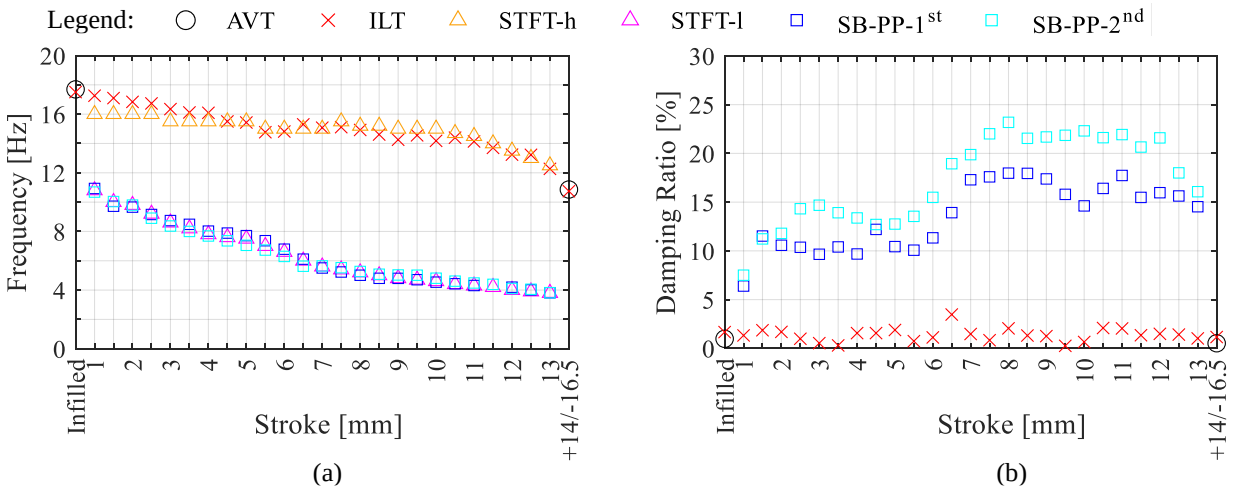

Figure 16. Longitudinal mode of the infilled mock-up: (a) resonant frequency and (b) damping ratio evolutions.

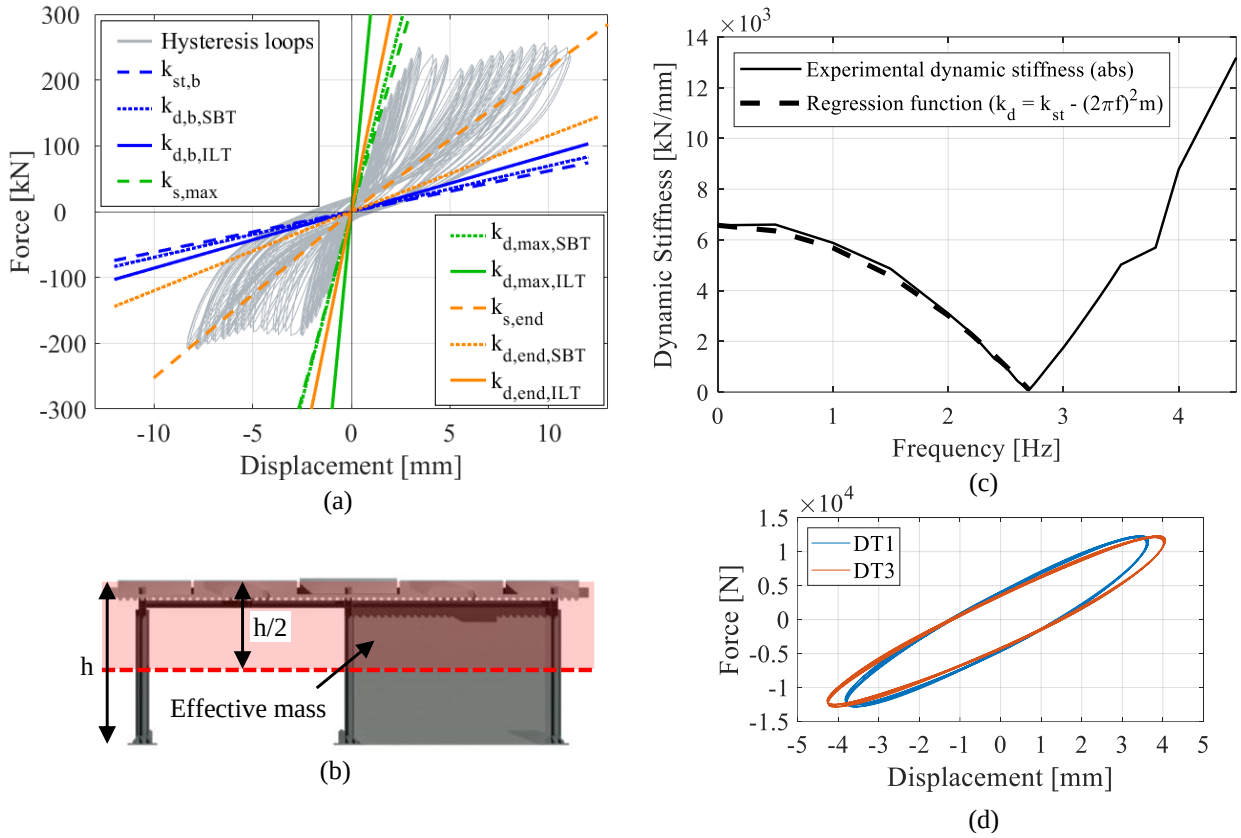

Figure 17. (a) stiffnesses overlapped to hysteresis loops, (b) hypotesys effective mass calculation, (c) experimental dynamic stiffness and regression function for the bare frame mass estimation, (d) example of steady hysteretic cycles for f = 2 Hz on the bare frame.

Table 4. Comparisons between mock-up static/secant and dynamic stiffnesses determined in different phases of the experimentation.

Experimental phase	Static/secant stiffness (k_{st} / k_s) [kN/mm]	Dynamic stiffness (k_d) [kN/mm]	
		ILT	SBT
Bare mock-up	$k_{st,b}$ = 6.20	$k_{d,b,ILT}$ = 8.59	$k_{d,b,SBT}$ = 6.95
Undamaged infills	$k_{s,max}$ = 101 (push) 112 (pull)	$k_{d,max,ILT}$ = 307.81	$k_{d,max,SBT}$ = 114.78
Completely damaged infills	$k_{s,end}$ = 22 (push) 25 (pull)	$k_{d,end,ILT}$ = 148.59	$k_{d,end,SBT}$ = 14.41

The dynamic stiffness of the mock-up is calculated in three crucial phases of the experimentation and results are listed in Table 4. Starting from the bare mock-up, Figure 17a (lines coloured in blue) shows that the dynamic stiffness calculated from SBTs ($k_{d,b,SBT}$) is slightly higher than the static one ($k_{st,b}$), and that calculated from ILTs (or AVTs since results are very similar) is even more high ($k_{d,b,ILT}$). Similar considerations stem from the analysis of dynamic stiffnesses calculated for the infilled mock-up at the beginning of CLTs (undamaged infills, lines coloured in green). For the infilled mock-up it is more appropriate to refer to the secant stiffness (k_s) instead of the static one (k_{st}) since the structure always exhibited a pronounced non-linear behaviour. It is noteworthy to observe that the dynamic stiffness calculated based on low-amplitude tests ($k_{d,max,ILT}$) is almost three times greater than the others. The same occurs at the end of tests when the dynamic stiffness obtained from ILT results (or AVT as well) is much higher with respect to the others. These results highlight the need of establishing suitable reduction coefficients for the estimation of the static stiffness of infilled structures based on dynamic test results, which is a very common practice when numerical models are adjourned and updated based on results of in-situ dynamic tests. Finally, it is worth observing that also in this case the non-stationary behaviour of the infilled structure subjected to high level of excitation lead to a very different dynamic stiffness values if calculated starting from low- (ILTs) or high-amplitude (SBTs) tests.

6 Conclusions

The paper offered some insights on the usefulness of vibration data for the damage detection in infilled frame structures. To this purpose, a comprehensive experimental campaign on an infilled steel-concrete composite laboratory

mock-up has been performed and the main results have been presented. In detail, quasi-static cyclic tests have been performed to induce a progressive damage to infills simulating an earthquake damage scenario; during the progressive damage of infills, the system identification is carried out on the basis of vibration records obtained from different dynamic test typologies characterised by different level of input excitation provided to the structure, addressing and discussing the possibility of detecting the infill damage by the analysis of the relevant acquired data. Dynamic tests on the bare and the undamaged system are also performed for comparisons.

From the analysis of cycle load test results it was evident that infills substantially increased the longitudinal stiffness of the mock-up, although a certain level of drift was needed to activate shear force transfer mechanisms and to reach the maximum values of secant stiffness. The stiffness increment was also proved by the increasing in the frequency values identified from dynamic tests performed after the infill construction. Moreover, resisting mechanisms of infills evolved with the drift values and became stable at high drifts, where the residual stiffness and damping were essentially due to friction forces developing through cracking. This was also proved by the crack pattern evolution on infills, which consisted at first in the formation of horizontal cracks, and then of diagonal cracks. At maximum imposed drift (4‰) infills were severely damaged, but they still contribute to the mock-up longitudinal stiffness.

Infill damage was also critically discussed with the aim of correlating the crack patterns with the infill mechanical property evolution. This was done summarizing the main mechanical and dynamic parameters obtained in crucial phases of the experimentation with the relevant observed damage. The formation of the first important infill damage (horizontal cracks) resulted in a strength and longitudinal secant stiffness reduction of the whole structure, while the subsequent formation of diagonal cracks was correlated to a slight strength increment, probably due to the activation of different resisting mechanisms within the infill panel, and to a further stiffness decrement. Even if the strength decay was not so high to be of concern, the stiffness decay was so significant as to suggest that safe use of the structure might be compromised, for issues related to the out of plane stability of infills. These critical analyses can be useful for practitioners and/or building owners in a decision-making process when the healthy status and the useability of infilled structures stroked by earthquakes must be evaluated.

For what concerns dynamic tests, the activation of non-linear phenomena had important consequences in the identification of the structural dynamics. Indeed, the longitudinal vibration mode frequencies obtained from ambient vibration or impact load tests are largely higher than those obtained from data of snap-back tests just after the release. However, the tracing of the frequency evolutions during the infill damage from both low- and high-amplitude vibration tests demonstrated to be an effective tool in the structural health monitoring of the laboratory mock-up, because it allowed to identify a damage activation through the detection of decay trends. Nevertheless, the observed frequency decays show an almost linear trend, and revealed unhelpful to individuate the specific phase in which the main damage occurred. On the contrary, the damping ratio evolution achieved from high amplitude tests (snap-back tests) show a trend that can be correlated to the beginning and evolution of the progressive infills damage.

General outcomes of the experimental research can be extended to real structures where the tracking of modal properties is commonly achieved through the execution of ambient vibration tests or through the analysis of data obtained from permanently installed structural health monitoring systems. In the latter case, the structural dynamic response due to both ambient and seismic excitations of different intensities can be available and the model parameters can be extracted adopting suitable strategies available in the literature, depending on the measured response and the input typology.

References

[1] Carden E.P., Fanning P. Vibration based condition monitoring: A review. Struct. Health Monit., 3, 355-377, 2004.

[2] Kong X., Cai C.S., Hu J. The state-of-the-art on framework of vibration-based structural damage identification for decision making. Appl. Sci., 7(5), 497, 2017.

[3] Nicoletti V., Arezzo D., Carbonari S., Gara F. Vibration-based tests and results for the evaluation of infill masonry walls influence on the dynamic behaviour of buildings: A review. Arch. Comput. Methods Eng., Forthcoming, 2022.

[4] Molinari M., Savadkoohi A.T., Bursi O.S., Friswell M.I., Zonta D. Damage identification of a 3D full scale steel-concrete composite structure with partial-strength joints at different pseudo-dynamic load levels. Earthq. Eng. Struct. Dyn., 38(10), 1219-1236, 2009.

[5] Yousefianmoghadam S., Song M., Mohammadi M.E., Packard B., Stavridis A., Moaveni B., Wood R.L. Nonlinear dynamic tests of a reinforced concrete frame building at different damage levels. Earthq. Eng. Struct. Dyn., 49(9), 924-945, 2020.

[6] Yousefianmoghadam S., Behmanesh I., Stavridis A., Moaveni B., Nozari A., Sacco A. System identification and modelling of a dynamically tested and gradually damaged 10-story reinforced concrete building. Earthq. Eng. Struct. Dyn., 47(1), 25-47, 2018.

[7] Yu E., Skolnik D., Whang D.H., Wallace J.W. Forced vibration testing of a four-story reinforced concrete building utilizing the nees@UCLA mobile field laboratory. Earthq. Spectra, 24(4), 969-995, 2008.

[8] Uebayashi H., Nagano M., Hida T., Tanuma T., Yasui M., Sakai S. Evluation of the structural damage of high-rise reinforced concrete buildings using ambient vibrations recorded before and after damage. Earthq. Eng. Struct. Dyn., 45, 213-228, 2016.

[9] Gara F., Arezzo D., Nicoletti V., Carbonari S. Monitoring the modal properties of an RC school building during the 2016 Central Italy seismic swarm. J. Struct. Eng. (ASCE), 147(7), 05021002, 2021.

[10] Moaveni B., He X., Conte J.P., Restrepo J.I., Panagiotou M. System identification study of a 7-story full-scale building slice tested on the UCSD-NEES shake table. ASCE J. Struct. Eng., 137(6), 705-717, 2010.

[11] Belleri A., Moaveni B., Restrepo J.I. Damage assessment through structural identification of a three-story large-scale precast concrete structure. Earthq. Eng. Struct. Dyn., 43(1), 61-76, 2014.

[12] Moaveni B., Stavridis A., Lombaert G., Conte J.P., Shing P.B. Finite-element model updating for assessment of progressive damage in a 3-story infilled RC frame. ASCE J. Struct. Eng., 139(10), 1665-1674, 2013.

[13] Zembaty Z., Kowalski M, Pospisil S. Dynamic identification of a reinforced concrete frame in progressive states of damage. Eng. Struct., 28(5), 668-681, 2006.

[14] Astroza R, Ebrahimian H, Conte JP, Restrepo JI, Hutchinson TC. Influence of the construction process and nonstructural components on the modal properties of a five-story building. Earthq. Eng. Struct. Dyn., 45(7), 1063-1084, 2016.

[15] Ji X., Fenves G., Kajiwara K., Nakashima M. Seismic damage detection of a full-scale shaking table test structure. ASCE J. Struct. Eng., 137(1), 14-21, 2011.

[16] Wang X., Hutchinson T.C. Evolution of modal characteristics of a mid-rise cold-formed steel building during construction and earthquake testing. Earthq. Eng. Strcut. Dyn., 49(14), 1539-1558, 2020.

[17] Chellini G., De Roeck G., Nardini L., Salvatore W. Damage detection of a steel-concrete composite frame by a multilevel approach: Experimental measurements and modal identification. Earthq. Eng. Struct. Dyn., 37(15), 1763-1783, 2008.

[18] Ventura CE, Schuster ND. Structural dynamic properties of a reinforced concrete high-rise building during construction. Canadian J. Civil Eng., 23(4), 950-972, 2011.

[19] Gara F., Carbonari S., Roia D., Balducci A., Dezi L. Seismic retrofit assessment of a school building through operational modal analysis and f.e. modelling. ASCE J. Struct. Eng., 147(1), 04020302, 2021.

[20] Gabbianelli G., Perrone D., Brunesi E., Monteiro R. Seismic acceleration and displacement demand profiles of non-structural elements in hospital buildings. Buildings, 10(12), 243, 1-19, 2020.

[21] Dolsek M., Fajfar P. Simplified non-linear seismic analysis of infilled reinforced concrete frames. Earthq. Eng. Struct. Dyn., 34(1), 49-66, 2005.

[22] Morandi P., Hak S., Milanesi R.R., Magenes G. In-plane/out-of-plane interaction of strong masonry infills: From cyclic tests to out-of-plane verifications. Earthq. Eng. Struct. Dyn., 2021.

[23] Furtado A., Rodrigues H., Varum H., Arede A. Mainshock-aftershock damage assessment of infilled RC structures. Eng. Struct., 175, 645-660, 2018.

[24] Manfredi G., Ricci P., Verderame G. Influence of infill panels and their distribution on seismic behaviour of existing reinforced concrete buildings. Open Constr. Build. Technol. J., 6(SS1), 236-253, 2012.

[25] Cavaleri L., Fossetti M., Papia M. Infilled frames: developments in the evaluation of cyclic behaviour under lateral loads. Struct. Eng. Mech., 21(4), 469-494, 2005.

[26] Akhlaghi M.M., Bose S., Mohammadi M.E., Moaveni B., Stavridis A., Wood R.L. Post-earthquake damage identification of an RC school building in Nepal using ambient vibration and point cloud data. Eng. Struct., 227, 111413, 2021.

[27] Furtado A., Vila-Pouca N., Varum H., Arede A. Study of the seismic response on the infill masonry walls of a 15-storey reinforced concrete structure in Nepal. Buildings, 9(2), 39, 2019.

[28] Yu H., Mohammed M.A., Mohammadi M.E., Moaveni B., Barbosa A.R., Stavridis A., Wood R.L. Structural identification of an 18-story RC building in Nepal using post-earthquake ambient vibration and lidar data. Front. Built. Environ., 3, 11, 2017.

[29] Gautam D. Ambient vibration measurements in representative buildings in Kathmandu Valley following the Gorkha earthquake. J. Perform. Constr. Facil., 32(3), 04018028, 2018.

[30] Barbosa A.R., Fahnestock L.A., Fick D.R., Gautam D., Soti R., Wood R., Moaveni B., Stavridis A., Olsen M.J., Rodrigues H. Performance of medium-to-high rise reinforced concrete frame buildings with masonry infill in the 2015 Gorkha, Nepal, earthquake. Earthq. Spectra, 33(S1), 197-218, 2017.

[31] Shah S.A.A., Khan J.S., Ali S.M., Shahzada K., Ahmad W., Shah J. Shake table response of unreinforced masonry and reinforced concrete elements of special moment resisting frame. Adv. Civ. Eng., 7670813, 2019.

[32] Moaveni B., Stavridis A., Lombaert G., Conte J.P., Shing P.B. Finite-element model updating for assessment of progressive damage in a 3-story infilled RC frame. J. Struct. Eng., 139(10), 1665-1674, 2013.

[33] Calò M., Malomo D., Gabbianelli G., Pinho R. Shake-table response simulation of a URM building specimen using discrete micro-models with varying degrees of detail. Bull. Earthq. Eng., 19(14), 5953-5976, 2021.

[34] Nicoletti V., Arezzo D., Carbonari S., Gara F. Dynamic monitoring of buildings as a diagnostic tool during construction phases. J. Build. Eng., 46, 103764, 2022.

[35] Nicoletti V, Arezzo D, Carbonari S, Gara F. Expeditious methodology for the estimation of infill masonry wall stiffness through in-situ dynamic tests. Constr. Build. Mat., 262, 120807, 2020.

[36] Ragni L., Dezi L., Dall'Asta A., Leoni G. HDR devices for the seismic protection of frame structures: Experimental results and numerical simulations. Earthq. Eng. Struct. Dyn., 38, 1199-1217, 2009.

[37] Imposa S., Lombardo G., Panzera F., Grassi S. Ambient vibrations measurements and 1D site response modelling as a tool for soil and building properties investigation. Geosciences, 8(3), 87, 2018.

[38] Al-Nimry H., Resheidat M., Al-Jamal M. Ambient vibration testing of low and medium rise infilled RC frame buildings in Jordan. Soil Dyn. Earthq. Eng., 59, 21-29, 2014.

[39] Moaveni B., Barbosa A.R., Conte J.P., Hemez F.M. Uncertainty analysis of system identification results obtained for a seven-story building slice tested on the UCSD-NEES shake table. Struct. Control Health Monit., 21(4), 466-483, 2014.

[40] Soyoz S., Taciroglu E., Orakcal K. Nigbor R., Skolnik D., Lus H., Safak E. Ambient and forced vibration testing of a reinforced concrete building before and after its seismic retrofitting. J. Struct. Eng., 139(10), 1741-1752, 2013.

[41] Aras F. Laboratory tests and vibration surveys for the mechanical properties of infill walls. J. Perform. Constr. Facil., 32(1), 04017117.

[42] Park S.A., Choi J.S., Min K.W. Dynamic characteristics for traditional wooden structure in Korea by using impact hammer test. Proceedings of 12th East Asia-Pacific Conference on Structural Engineering and Construction, EASEC12, 14, 477-484, 2011.

[43] Cunha A., Caetano E., Delgado R. Dynamic tests on large cable-stayed bridge. J. Bridge. Eng., 6(1), 54-62, 2001.

[44] Lu Y., Song J., Xiong F., Dai K., Zhou G., Wei M., Zhang S. Simplified procedures for seismic design verification and evaluation of lead rubber bearing base-isolated buildings based on free-vibration response. Struct. Des. Tall Spec. Build., 29(12), art. numb. e1751, 2020.

[45] Dall'Asta A., Leoni G., Micozzi F., Gioiella L., Ceccolini N., Ragni L. The new Camerino University research center: Design of the base-isolated buinding and dynamic testing. Proceedings of the 8th Int. Conf. on Comp. Methods in Struct. Dyn. and Earthq. Eng., COMPDYN 2021, art. numb. 174550, 2021.

[46] Peeters B., De Roeck G. Stochastic system identification for operational modal analysis: A review. J. Dyn. Syst. Meas. Contr., 123(4), 659-667, 2001.

[47] Van Overschee P., De Moor B. Subspace identification for linear systems: Theory-Implementation-Applications. Norwell, MA, Kluwer Academic Publishers, 2012.

[48] Chopra A.K. Dynamic of structures – Theory and applications to earthquake engineering. Fifth edition, US, Pearson Education, 2019.

[49] Ditommaso R., Mucciarelli M., Ponzo F.C. Analysis of non-stationary structural systems by using a band-variable filter. Bull. Earthq. Eng., 10(3), 895-911, 2012.

[50] Ceravolo R., Matta E., Quattrone A., Zanotti Fragonara L. Amplitude dependence of equivalent modal parameters in monitored buildings during earthquake swarms. Earthq. Eng. Struct. Dyn., 46(14), 2399-2417, 2017.

[51] Markulak D., Radic I., Sigmund V. Cyclic testing of single bay steel frames with various types of masonry infill. Eng. Struct., 51, 267-277, 2013.

[52] Morandi P., Hak S., Milanesi R., Magenes G. In-plane/out-of-plane interaction of strong masonry infills: From cyclic tests to out-of-plane verifications. Earthq. Eng. Struct. Dyn., 51(3), 648-672, 2022.

[53] Crisafulli F.J. Seismic behaviour of reinforced concrete structures with masonry infills. Ph.D. Thesis, University of Canterbury, Christchurch, New Zealand, 1997.

[54] Asteris P.G., Cotsovos D.M., Chrysotomou C.Z., Mohebkhah A., Al-Chaar G.K. Mathematical micromodeling of infilled frames: State of the art. Eng. Struct., 56, 1905-1921, 2013.

[55] Mucedero G., Perrone D., Brunesi E., Monteiro R. Numerical modelling and validation of the response of masonry infilled rc frames using experimental testing results. Buildings, 10(10), 1-30, 182, 2020.

[56] Stafford Smith B. Behaviour of square infilled frames. ASCE J. Struct. Div., 92, 381-403, 1966.

[57] Al-Chaar G. Evaluating strength and stiffness of unreinforced masonry infill structures. Rep. No. ERDC/CERL TR-02-1, U.S. Army Corps of Engineers, Champaign, IL, USA, 2022.

[58] Zonta D., Elgamal A.W., Fraser M., Priestly M.J.N. Analysis of change in dynamic properties of a frame-resistant test building. Eng. Struct., 30(1), 183-196, 2008.